Available online at www.sciencedirect.com
ScienceDirect
Ore Geology Reviews 31 (2007) 319–336
ORE GEOLOGY REVIEWS
www.elsevier.com/locate/oregeorev

Rare earth element geochemistry of the Woxi W–Sb–Au deposit, Hunan Province, South China

Xuexiang Gu [a,b,*], Oskar Schulz [c], Franz Vavtar [c], Jianming Liu [d], Minghua Zheng [e], Shaohong Fu [b]

[a] College of Earth Sciences and Resources, China University of Geosciences, Beijing 100083, People's Republic of China
[b] Institute of Geochemistry, Chinese Academy of Sciences, Guiyang 550002, People's Republic of China
[c] Institut für Mineralogie und Petrographie, Universität Innsbruck, A-6020 Innsbruck, Austria
[d] Institute of Geology and Geophysics, Chinese Academy of Sciences, Beijing 100101, People's Republic of China
[e] College of Earth Sciences, Chengdu University of Technology, Chengdu 610059, People's Republic of China

Received 20 March 2003; accepted 20 January 2005
Available online 2 June 2006

Abstract

The Woxi W–Sb–Au deposit in Hunan, South China, is hosted by Proterozoic metasedimentary rocks, a turbiditic sequence of slightly metamorphosed (greenschist facies), gray-green and purplish red graywacke, siltstone, sandy slate, and slate. The mineralization occurs predominantly (>70%) as stratabound/stratiform ore layers and subordinately as stringer stockworks. The former consists of rhythmically interbedded, banded to finely laminated stibnite, scheelite, quartz, pyrite and silty clays, whereas the latter occurs immediately beneath the stratabound ore layers and is characterized by numerous quartz+pyrite+gold+scheelite stringer veins or veinlets that are typically either subparallel or subvertical to the overlying stratabound ore layers. The deposit has been the subject of continued debate in regard to its genesis. Rare earth element geochemistry is used here to support a sedimentary exhalative (sedex) origin for the Woxi deposit. The REE signatures of the metasedimentary rocks and associated ores from the Woxi W–Sb–Au deposit remained unchanged during post-depositional processes and were mainly controlled by their provenance. The original ore-forming hydrothermal fluids, as demonstrated by fluid inclusions in quartz from the banded ores, are characterized by variable total REE concentrations (3.5 to 136 ppm), marked LREE enrichment (La_N/Yb_N=28–248, ∑LREE/∑HREE=16 to 34) and no significant Eu-anomalies (Eu/Eu*=0.83 to 1.18). They were most probably derived from evolved seawater that circulated in the clastic sediment pile and subsequently erupted on the seafloor. The bulk banded ores are enriched in HREE (La_N/Yb_N=4.6–11.4, ∑LREE/∑HREE=3 to 14) and slightly depleted in Eu (Eu/Eu*=0.63 to 1.14) relative to their parent fluids. This is interpreted as indicating the influence of seawater rather than a crystallographic control on REE content of the ores. Within a single ore layer, the degree of HREE enrichment tends to increase upward while the total REE concentrations decrease, reflecting greater influence and dilution of seawater. There is a broad similarity in chondrite-normalized REE patterns and the amount of REE fractionation of the banded ores in this study and exhalites from other sedex-type polymetallic ore deposits, suggesting a similar genesis for these deposits. This conclusion is in agreement with geologic evidence supporting a syngenetic (sedex) model for the Woxi deposit.

Keywords: Rare earth element geochemistry; Stratiform W–Sb–Au deposit; Sedimentary exhalation; Ore genesis; Woxi; South China

* Corresponding author. Current address: College of Earth Sciences and Resources, China University of Geosciences, Beijing, 100083, People's Republic of China.
E-mail address: gxx@cdut.edu.cn (X. Gu).

0169-1368/$ - see front matter © 2006 Elsevier B.V. All rights reserved.
doi:10.1016/j.oregeorev.2005.01.003

1. Introduction

A number of metasedimentary rock-hosted stratiform and/or stratabound W–Sb–Au, W–Au, Sb–Au, Sb, and Au deposits occur within the Jiangnan Proterozoic orogenic belt at the southeastern margin of the Yangtze Craton, South China. With the total proved ore reserves of 250,000 t WO_3, 1.67 Mt Sb, and 42 t Au (Luo et al., 1996), and average grades ranging from 0.2% to 0.8% WO_3, 2% to 6% Sb and 5 to 10 g/t Au, the Woxi W–Sb–Au deposit is one of the largest stratiform polymetallic deposits in this metallogenic belt. In addition, the Woxi deposit represents one of few documented cases where the three metals, W, Sb, and Au, are all present on a large-scale within a single deposit.

Regarding the relative timing of the mineralization, its relationship to metamorphism and tectonic deformation and the genesis of ore precipitation, the deposit has been the subject of continued debate. Early workers considered the mineralization to be a distal part of magmatic hydrothermal systems and proposed that magmas were the source for most fluid components and metals (see summaries by Zhang, 1980, 1989). Later, some researchers argued that the magmatic hypothesis does not explain the lack of igneous activity in the mining district and suggested that major fluid components were derived from regional metamorphism of supercrustal rocks (Luo et al., 1984; Luo, 1990; Ma, 1991; Ma and Liu, 1992; Liu et al., 1993; Luo, 1994) or post-metamorphic meteoric water circulation (Zheng, 1989; Yang, 1985, 1992). Metals, sulphur, and silica were scavenged from sedimentary "source beds" (e.g., Ma, 1991; Liu et al., 1993) at depth and were deposited in chemically favorable environments as the fluids ascended. Based on comprehensive studies on the ore mineralogy and textures, nature of ore layering, geochemistry of trace elements, fluid inclusions, and sulphur isotopes, Gu et al. (2002a, 2003, 2004) and Schulz et al. (2002) most recently proposed a syngenetic model in which the mineralization formed by exhalative hot spring activity, whereby convective seawater percolated through the sediment pile and subsequently precipitated the ores on the seafloor.

The application of rare earth element (REE) geochemistry has been widely used to investigate petrogenetic problems of igneous and metamorphic rocks (see summaries by Haskin, 1984; McKay, 1989; Grauch, 1989), to identify provenances and tectonic settings of sedimentary rocks (e.g., Bhatia, 1985; Taylor and McLennan, 1985; McLennan, 1989; McLennan et al., 1990, 1993; Gu, 1994; McLennan et al., 1995; Taylor and McLennan, 1995; Gu et al., 2002b), to delineate interactions between rocks and fluids, particularly in hydrothermal fluids (e.g., Klinkhammer et al., 1994; Mills and Elderfield, 1995a,b; Van Middlesworth and Wood, 1998; German et al., 1999; Savelli et al., 1999; Sherrell et al., 1999) and, thus, to provide constraints on ore formation processes (e.g., Lottermoser, 1989a,b, 1992; Parr, 1992; Siva Siddaiah et al., 1994; Bierlein, 1995; Davies et al., 1998). The purposes of this paper are to outline the REE geochemistry of ores and associated host rocks, as well as ore-forming fluids, in the Woxi deposit, to compare these data with both active and ancient hydrothermal deposits, and to evaluate the potential of REE signatures in constraining ore genesis.

2. Regional geologic framework

South China consists of two complex Terranes, the Yangtze Craton to the NW and the Cathaysia Block to the SE (Fig. 1a). Collision between the Yangtze Craton and the Cathaysia Block occurred during Middle–Late Proterozoic times (Li et al., 1995; Chen and Jahn, 1998; Gu et al., 2002b) and led to uplift of the Jiangnan orogenic belt. The Woxi W–Sb–Au deposit is located in the western segment of this Proterozoic orogenic belt, approximately 200 km W of the capital city of Hunan Province, Changsha.

The stratigraphy near the Woxi mine consists of Middle–Upper Proterozoic basement deposited in a continental back arc basin (Gu et al., 2002b) and unconformably overlying Cretaceous molasse conglomerates (Figs. 1b and 2). The Middle Proterozoic Lengjiaxi Group (Pt_2ln) occurs mainly in the SW and SE parts of the mining district, whereas the Upper Proterozoic Banxi Group (Pt_3bn), including the Madiyi (Pt_3bnm) and Wuqiangxi (Pt_3bnw) Formations, dominates in the middle and northern parts of the orefield. The Madiyi and Wuqiangxi Formations are separated by the E-striking Woxi thrust fault. W–Sb–Au mineralization is confined to the middle to upper horizons of the Madiyi Formation in the footwall of the thrust.

Fig. 1. (a) Sketch map showing plate tectonics of South China and the location of the Woxi mine (modified from Gu et al., 2002b). (b) Sketch map showing structural features of the Woxi ore mine and its adjacent region. Also shown is a typical northeast–southwest section of the Woxi deposit (simplified after Luo et al., 1996).

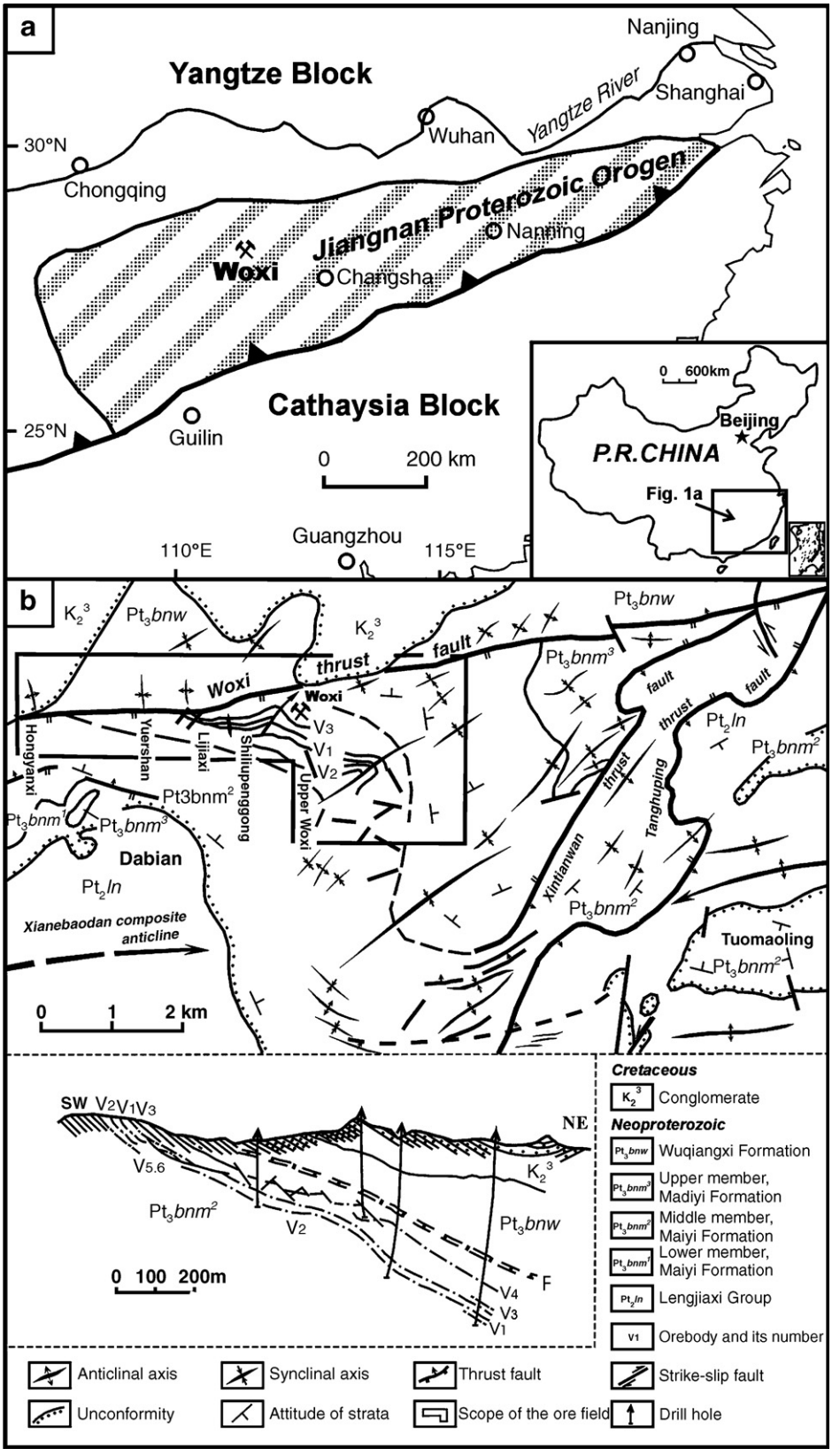
a
Yangtze Block
Nanjing
Shanghai
Yangtze River
Wuhan
30°N
Chongqing
Jiangnan Proterozoic Orogen
Nanning
Woxi
Changsha
Cathaysia Block
25°N
Guilin
0 200 km
0 600km
Beijing
P.R.CHINA
Fig. 1a
110°E
Guangzhou
115°E
b
K_2^3
Pt_3bnw
fault
thrust
Woxi
Pt_3bnm^3
Pt_2ln
Pt_3bnm^2
Hongyanxi
Yuershan
Lijiaxi
Shilupenggong
Upper Woxi
V3
V1
V2
Pt3bnm²
Pt_3bnm^1
Dabian
Tanghuping
Xintianwan
Xianebaodan composite anticline
Tuomaoling
0 1 2 km
SW V2V1V3
NE
V5.6
F
0 100 200m
Cretaceous
Conglomerate
Neoproterozoic
Wuqiangxi Formation
Upper member, Madiyi Formation
Middle member, Maiyi Formation
Lower member, Maiyi Formation
Lengjiaxi Group
Orebody and its number
Anticlinal axis
Synclinal axis
Thrust fault
Strike-slip fault
Unconformity
Attitude of strata
Scope of the ore field
Drill hole

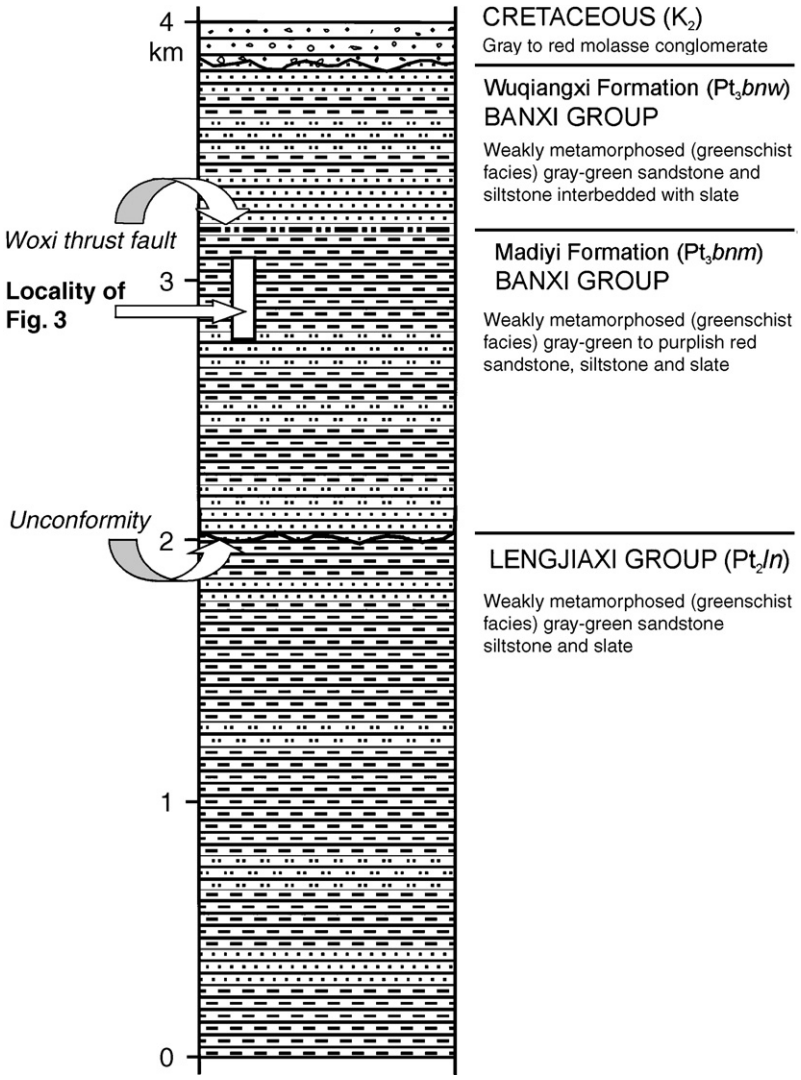

Fig. 2. Stratigraphic column of the Woxi mine (compiled after Liu et al., 1993; Luo et al., 1996; Gu et al., 2002a).

Tectonically, the Woxi mine lies within the northern limb of a major complex, faulted, dome-shaped, and east-trending anticline, the Xianebaodan (Fig. 1b), which is considered to be product of the S–N crustal shortening during the Dong'an orogeny at ~1 Ga (Luo et al., 1996). South–north sinistral strike slip movement during the Late Proterozoic Xuefeng Orogeny (~0.8 Ga) resulted in the overprinting of numerous mesoscopic, NNE- to NE-trending folds on the northern limb of the Xianebaodan anticline and the formation of related NE-trending and moderately SE-dipping faults (e.g., the Xintianwan and Tanghuping thrust faults, Fig. 1b). In the deposit area, the most notable fault structure is the Woxi thrust fault, which strikes roughly E and dips ~30° to N, with a strike length of approximately 20 km and a dip extent of over 2 km. According to Luo et al. (1996), this thrust fault initially formed during the Dong'an Orogeny and was reactivated during the Xuefeng Orogeny.

Igneous activity is lacking in the Woxi mine district. Regionally, the nearest granodioritic intrusive rocks of the Caledonian (~390 Ma) and Yanshanian (190 to 90 Ma) ages occur near Yiyang City, ca. 120 km E from the mine district (Luo et al., 1996).

3. Geology of the deposit

The mine district is subdivided into five ore blocks. From west to east, these are the Hongyanxi, Yuershan, Lijiaxi, Shiliupenggong, and Upper Woxi (Fig. 1b).

The W–Sb–Au mineralization encompasses two principle styles characterized by varying locations, mineralogy, textures, and the relationships to the host rocks, i.e., the stratabound banded ore layers and the stockworks.

The stratabound mineralization accounts for >70% of the total proven ore reserves and comprises 9 banded ore layers (orebodies V1–V9) localized within different stratigraphic horizons of the Madiyi Formation (Figs. 1b, 2 and 3). Recent exploration has revealed three additional blind ore layers below the orebody V6 (B1–B3). Orebodies V1–V4 in the middle part of the mineralized sequence comprise the main stratabound mineralization, whereas orebodies V5–V9 and blind ore layers B1–B3 are small, discontinuous, and economically less important. The ore layers strike approximately E and dip 20° to 35° to the north. They are typically sheet-like, with a strike length of 40 to 350 m, a dip extent up to 3500 m (generally 300 to 2300 m), and a true thickness ranging from 0.2 to 1.5 m. The ores consist of rhythmically interbedded, massive to laminated gold-bearing quartz, well-laminated stibnite, scheelite, pyrite and silty clays (quartz silt, sericite and chlorite) with, locally, minor to trace amounts of arsenopyrite, chalcopyrite, sphalerite, galena, wolframite, carbonates and barite (Fig. 4a–b, e–f). The ore layering and/or lamination are strictly parallel to the

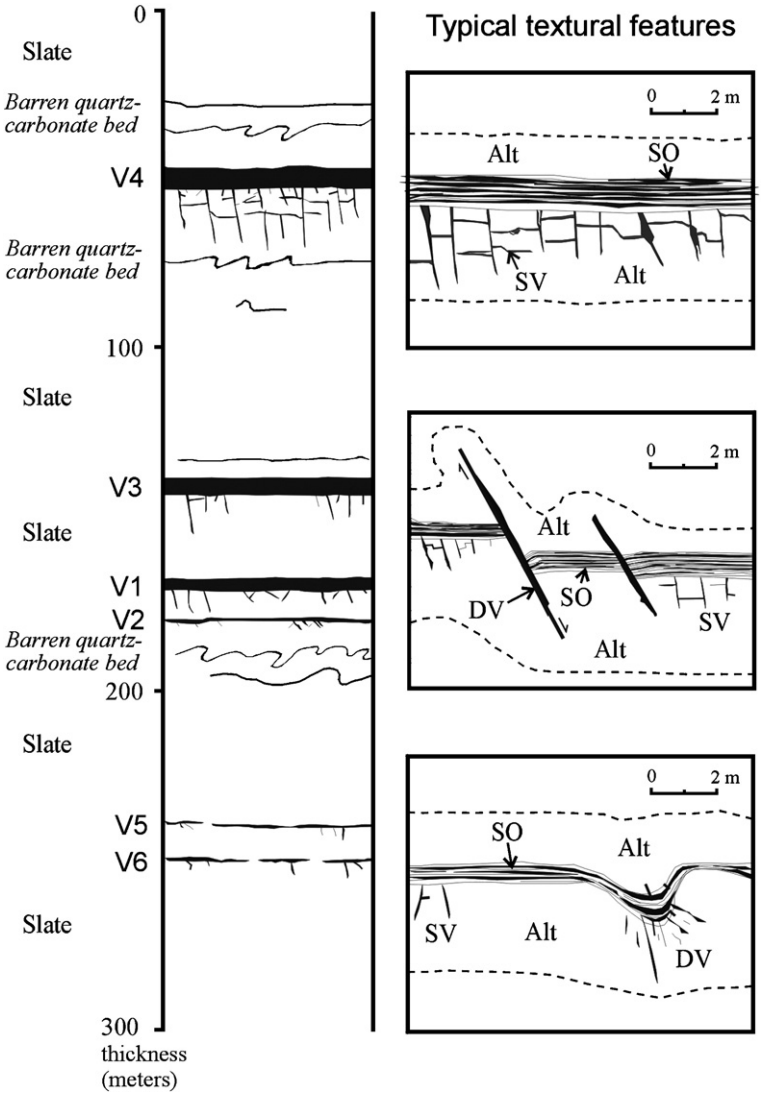

Fig. 3. Generalized stratigraphic section showing the location of orebodies V1–V6 and typical textural relations between stratiform ores (SO), stringers (SV), discordant veins (DV), and alteration blankets (Alt).

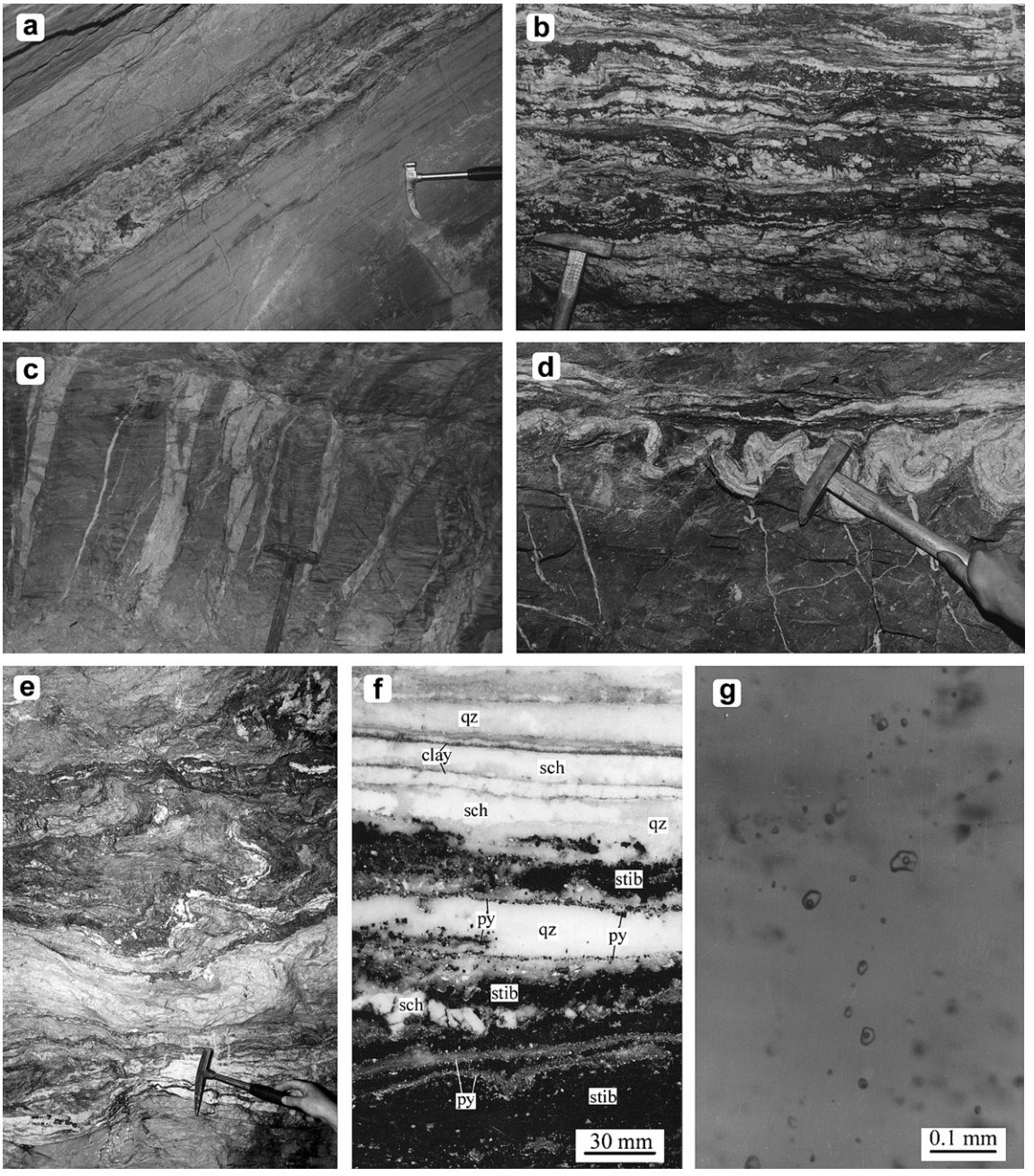

Fig. 4. (a) Bedding-parallel, stratiform ore layer, with planar and conformable contacts with both the overlying and underlying host slates. Note the relatively thicker alteration blanket (light gray) of the footwall than the hanging-wall. (b) Typical, close views of stratiform ore layer: fine layering of stibnite (black), quartz–scheelite (white), and silty clays (gray). (c) Quartz–scheelite stringer veins and veinlets (white) within the footwall alteration blanket (gray) beneath stratiform ores. (d) Small-scale folds of barren quartz–carbonate layers (white) bounded above and below by undisturbed metasediments, indicating soft-sediment deformation. (e) Stratiform ores illustrating soft-sediment deformation. Note the relatively undeformed footwall and hanging-wall metasedimentary rocks. (f) Fine layering of stibnite (stib), pyrite (py)-rich clay, quartz (qz), and scheelite (sch) under reflected light. The scheelite laminae are partly fractured. Polished section. (g) Typical, primary, liquid-rich, two-phase (liquid+vapour) fluid inclusions in quartz bands. Doubly polished section.

stratification of the host metasedimentary rocks; thus, the stratabound mineralization is also stratiform in character.

Contacts between the banded ore layers and the overlying and underlying host rocks are sharp and conformable, which is partly due to shearing along the

contacts. In places, both ore layers and host metasedimentary rocks are folded and sheared. Locally, breccias of possibly synsedimentary origin occur within the ore layers and take the form of dm-thick lenses. These breccias contain angular clasts of quartz, quartz–scheelite, and quartz–stibnite as well as host rock lithology, and are cemented predominantly by stibnite, quartz, and pyrite. In the immediate vicinity of the metasedimentary rocks hosting stratiform mineralization, several beds of barren quartz and carbonate (ankerite–calcite±dolomite) are present as mm- to cm-thick interbeds and traceable over the distance of tens to hundreds of m along bedding (Fig. 3). Structures of soft-sediment deformation due to slumping and synsedimentary sliding are well developed within both banded ores and barren quartz–carbonate beds, where small-scale folds are bounded above and below by undisturbed metasediments (Gu et al., 2002a, 2003; Fig. 4d–e).

The stockwork mineralization accounts for about 25% of the total ore reserves at Woxi. It occurs in the footwall slate below the stratiform ore layers and is restricted to a 3- to 10-m-thick zone adjacent to the stratiform ores (Figs. 3 and 4c). The stockworks are characterized by numerous quartz+pyrite±gold± scheelite stringer veins or veinlets that typically are either subparallel or subvertical to the overlying stratiform quartz+gold+scheelite+stibnite beds. Except for pyrite and trace amounts of arsenopyrite, sulphide minerals commonly are absent in the vein ores. The stockwork zone generally takes the form of lenses or wedges, with a strike length of 20 to 60 m and a dip extent of 40 to 120 m. Individual stringer veins are planar, 0.5 to 5 cm wide, 1 to 5 m long, and typically spaced 5 to 50 cm apart. They often exhibit textures indicative of hydraulic fracturing and open-space filling. Locally, vein textures are characterized by banded crustiform quartz–scheelite–pyrite often showing growth zoning on a fine scale. Contacts between the stringers and the walls are sharp. These stringer veins are interpreted to represent feeder zones in a sedimentary exhalative system (see discussion below).

In addition to the stratiform and stockwork mineralization described above, there exist locally some discordant veins and veinlets occurring as variably oriented, planar to irregular cleavage and fissure fillings of quartz±scheelite±stibnite±gold±carbonate, both above and below the stratiform ore layers and often crosscutting the stratiform ores (Fig. 3). The veins and veinlets vary from several mm to over 1 m across and extend for several cm to a few tens of m along strike. These discordant veins are best developed near the cores of local folds, suggesting a syn- to post-deformational origin (remobilization) during folding and cleavage development.

Ore mineralogy of the Woxi deposit consists predominantly of stibnite, scheelite, native gold, and pyrite, with minor wolframite, arsenopyrite, sphalerite, and galena, and trace amounts of tetrahedrite, bournonite, boulangerite, gersdorffite, chalcopyrite, and aurostibite. Gangue minerals consist predominantly of quartz, with subordinate to minor amounts of calcite, dolomite, ankerite, siderite, barite, sericite, and chlorite. Supergene minerals including goethite, lepidocrocite, valentinite, senarmontite, cervantite, malachite, azurite, cuprite, and covellite are rare and only locally observed in the uppermost parts of the deposit.

The wall rock alteration at Woxi occurs as semi-conformable, tabular blankets that range from 0.2 to 2 m, locally up to 10 m, in thickness along the entire length of the orebodies. The footwall blanket is generally more intensely altered and somewhat thicker than the hanging-wall blanket (Figs. 3 and 4a). Contacts between the alteration zone and the wall rocks are typically gradational. The alteration blanket, informally termed the “bleached zone” by the mining geologists, is light gray, yellowish white, or pale red, and is dominated by a quartz–sericite–chlorite–pyrite±carbonate (ankerite and/or dolomite) assemblage. Trace amounts of disseminated tourmaline and barite locally occur in the alteration assemblage. In terms of wall rock alteration mineralogy, there is no distinct difference between stockwork and stratiform mineralization. The alteration is typically pervasive or patchy, though microfissure fillings of quartz+pyrite±dolomite±chlorite are in places recognizable. Sedimentary structures such as banding and fine laminations are well preserved in the altered rocks. No distinct alteration zoning has been observed, though intense quartz–sericite–pyrite alteration seems to occur more commonly proximal to the ore beds in the footwall.

4. Sampling and analytical methods

Sampling was carried out on fresh exposures in underground workings within the mine. Samples for the REE analyses in this study include five main groups: (1) fresh, unaltered, purplish red slates representing the host rock lithology; (2) altered (“bleached”), light gray to yellowish white slates from the alteration blanket, both underlying and overlying stratiform ore layers; (3) banded to finely laminated quartz–stibnite–scheelite ores with a similar mineral proportion (45% to 50% quartz, ~40% stibnite, 5% to 10% scheelite, and <1% pyrite

+clays); (4) individual quartz and clay bands within the stratiform ores; and (5) quartz mineral separates from the banded ores for the determination of REE in fluid inclusions. Petrographic studies on doubly polished section have shown that the fluid inclusions in quartz for the REE analysis are dominated (>95%) by primary, liquid-rich inclusions in both number and volume (Fig. 4g). They typically have rounded or negative crystal shapes and were aligned along growth zones in quartz. Therefore, the fluids extracted from the inclusions are thought to represent the primary ore-forming saline solutions.

Analyses were performed using a Finningan MAT ELEMENT high resolution inductively coupled plasma spectrometer (ICP–MS) at the Institute of Geochemistry, Chinese Academy of Sciences, following the methods of Balaram et al. (1995) and Wu et al. (1996). For the REE analysis of fluid inclusions, the crush-leach technique described by Ghazi et al. (1993) and Su et al. (1998) was used. Precision and accuracy for standards GSR-3 and JG-2, as determined by ICP–MS, are within 5% to 10%.

5. Results

Table 1 shows the REE data of 26 samples from the Woxi deposit, including 4 unaltered slates, 8 altered slates, 7 bulk banded/laminated ores, 2 quartz bands and 2 clay bands from the bulk ores, and 3 samples of fluid inclusions in quartz separates from the banded ores. The chondrite-normalized REE patterns of these samples are shown in Fig. 5. For comparative purposes and visual clarity, bulk ores, quartz and clay bands as well as fluid inclusions are also normalized to the average unaltered slate of the deposit as shown in Fig. 6.

Unaltered and altered slates in the deposit are essentially indistinguishable in terms of the absolute concentrations, characteristic parameters, and chondrite-normalized patterns of rare earth elements (Table 1; Fig. 5a–b), comparable with the regional Madiyi Formation slates (Gu et al., 2002b) and typical post-Archean shales such as PAAS and NASC (Gromet et al., 1984; Taylor and McLennan, 1985). The REE-patterns are uniform, with LREE enrichment (La_N/Yb_N = 5.6 to 7.7), ∑LREE/∑HREE = 5.8 to 8.7), flat HREE (Gd_N/Yb_N = 1.1 to 1.5), significant negative Eu-anomalies (Eu/Eu∗ = 0.62 to 0.81), and no Ce anomalies.

Except for one sample (WX20-5-1) that has a high total REE concentration (201 ppm) comparable with the host slates, the bulk banded ore samples in general have relatively low but variable ∑REE on the order of 4 to 82 ppm. Their chondrite-normalized REE patterns are comparable overall with both the unaltered and altered host rocks (Fig. 5c–e), although the characteristic parameters such as Eu/Eu* (0.63 to 1.14, typically < 1), Nd_N/Yb_N (2.0 to 4.5), La_N/Yb_N (4.6 to 11.4), La_N/Sm_N (2.8 to 6.5) and ∑LREE/∑HREE (3 to 14) are somewhat more variable (Table 1). Samples WX24-2 and WX24-4 are slightly U-shaped with weak enrichment of HREE (Fig. 5e). Within a single ore layer, in detail, samples from the lower parts tend to have a higher ∑REE and higher ratios of Nd_N/Yb_N, La_N/Yb_N, and ∑LREE/∑HREE than those from the upper parts in spite of their similar mineralogies (Fig. 5c–e; Table 1). In terms of the variation in Eu anomalies, the Eu/Eu* values of two data sets (samples WX20-6/WX20-7 and WX20-5-1/WX20-5-2; Fig. 5c and d) increase upward (from 0.68 to 1.14 and from 0.70 to 0.98, respectively; Table 1), while Eu/Eu* of the other data set (samples WX24-4/WX24-2; Fig. 5e) almost remains unchanged. On the slate-normalized plot (Fig. 6a), the bulk banded ores show relatively flat profiles, although both slightly HREE-enriched (samples WX20-7 and WX20-5-2) and slightly HREE-depleted (sample WX24-4) patterns are also noted in some samples.

Two samples of quartz bands have low to moderate ∑REE on the order of 6 to 28 ppm. Their chondrite- and slate-normalized patterns are virtually identical to the bulk-banded ores from which they were separated, and show a slightly U-shaped form (Figs. 5f and 6b). Two clay bands from the banded ore have high total REE concentrations (183 to 300 ppm) and exhibit similar REE-patterns to the host metapelites (Figs. 5g and 6b), suggesting a terrigenous origin.

The REE geochemistry of fluid inclusions in quartz from the banded ore is characterized by a relatively uniform chondrite-normalized REE-pattern (Fig. 5h), with variable ∑REE (3.5 to 136 ppm), marked LREE enrichment (La_N/Yb_N = 28 to 248, ∑LREE/∑HREE = 16 to 34), insignificant Eu-anomalies (Eu/Eu* = 0.83–1.18), and indistinct to slightly positive Ce-anomalies (Ce/Ce* = 0.87–1.42). When normalized against the average slate (Fig. 6c), the fluids exhibit significant HREE depletion and relatively flat LREE.

6. Discussion

6.1. Geologic evidence for ore genesis

Several lines of geological evidence at Woxi suggest a syngenetic origin (Gu et al., 2002a; Schulz et al., 2002; Gu et al., 2003). One of the most striking features of the deposit is that the stratiform ore layers are confined to definite horizons in the middle to upper parts of the

Table 1
Rare earth element concentrations (ppm) of rocks, ores, and fluid inclusions in quartz from the Woxi deposit

Sample	La	Ce	Pr	Nd	Sm	Eu	Gd	Tb	Dy	Ho	Er	Tm	Yb	Lu	SREE	Eu/Eu*	Ce/Ce*	NdN/YbN	LaN/YbN	LaN/SmN	GdN/YbN	SLREE/SHREE
Purplish red slate (unaltered)																						
WX20-9	39.32	82.26	9.61	34.35	6.63	1.34	5.52	0.87	5.43	0.86	3.09	0.47	3.43	0.52	193.69	0.68	0.99	3.49	7.74	3.73	1.30	8.53
WX20-2	33.69	70.97	8.21	29.24	5.60	1.18	4.70	0.75	4.69	0.73	2.82	0.46	3.35	0.53	166.89	0.70	1.00	3.05	6.80	3.79	1.14	8.20
WX20-1	36.77	76.46	9.06	32.09	6.35	1.30	5.16	0.72	5.09	0.77	2.82	0.46	3.28	0.50	180.84	0.69	0.98	3.41	7.57	3.64	1.28	8.55
WX28-1	44.31	92.16	10.77	36.95	7.59	1.60	6.58	1.00	6.74	1.02	3.80	0.57	3.98	0.60	217.66	0.69	0.99	3.24	7.53	3.67	1.34	7.90
"Bleached" slate (altered)																						
WX9-4	19.94	40.83	4.73	17.58	4.27	1.15	4.40	0.68	4.16	0.60	2.18	0.31	2.34	0.38	103.55	0.81	0.98	2.62	5.75	2.94	1.52	5.81
WX20-8	39.22	81.35	9.51	34.21	6.56	1.33	5.17	0.77	5.25	0.84	3.06	0.46	3.52	0.49	191.73	0.70	0.99	3.39	7.52	3.77	1.19	8.74
WX20-4	29.53	60.18	7.11	25.06	5.00	1.04	3.86	0.53	3.61	0.58	2.30	0.37	2.99	0.46	142.61	0.72	0.97	2.93	6.68	3.71	1.05	8.64
WX20-3	33.57	70.15	8.36	29.78	5.68	1.28	4.88	0.74	4.68	0.74	2.67	0.43	3.08	0.49	166.54	0.74	0.98	3.37	7.36	3.72	1.28	8.33
WX24-11	22.88	48.70	5.61	20.22	4.31	0.84	3.90	0.64	4.12	0.63	2.38	0.36	2.78	0.42	117.77	0.62	1.01	2.54	5.57	3.34	1.14	6.68
WX28-2	33.61	69.91	8.19	29.55	6.02	1.26	5.02	0.73	5.21	0.77	2.77	0.43	3.27	0.48	167.20	0.70	0.99	3.15	6.95	3.51	1.24	7.89
WX28-3	30.30	64.38	7.39	26.84	5.41	1.27	4.42	0.67	4.72	0.70	2.63	0.41	3.06	0.46	152.66	0.80	1.01	3.06	6.70	3.52	1.17	7.87
WX28-10	35.61	75.08	8.77	29.94	5.78	1.31	5.26	0.81	5.22	0.81	2.82	0.42	3.30	0.49	175.60	0.73	1.00	3.16	7.28	3.88	1.29	8.11
Banded quartz–scheelite–stibnite ore																						
WX20-7	2.56	5.16	0.60	2.12	0.54	0.26	0.88	0.14	1.02	0.12	0.42	0.06	0.38	0.08	14.32	1.14	0.98	1.95	4.56	2.98	1.87	3.55
WX20-6	17.33	34.03	3.95	14.36	2.87	0.57	2.26	0.34	2.29	0.35	1.29	0.21	1.54	0.24	81.62	0.68	0.96	3.25	7.61	3.80	1.19	8.53
WX20-5-2	2.76	5.38	0.62	2.15	0.62	0.22	0.78	0.11	0.70	0.10	0.33	0.05	0.35	0.06	14.21	0.98	0.97	2.14	5.31	2.82	1.81	4.67
WX20-5-1	40.33	84.98	10.01	35.99	7.07	1.44	5.62	0.84	5.53	0.86	3.22	0.52	3.70	0.55	200.66	0.70	0.99	3.40	7.37	3.59	1.23	8.56
WX24-2	1.06	1.95	0.21	0.62	0.10	0.02	0.07	0.01	0.07	0.01	0.05	0.01	0.08	0.01	4.25	0.63	0.98	2.87	9.55	6.48	0.70	12.98
WX24-4	2.91	6.08	0.69	2.23	0.42	0.07	0.25	0.03	0.20	0.03	0.13	0.02	0.17	0.04	13.28	0.67	1.01	4.49	11.37	4.34	1.18	14.00
WX28-4	0.98	1.83	0.19	0.67	0.15	0.04	0.14	0.02	0.09	0.02	0.05	0.01	0.07	0.02	4.28	0.78	0.98	3.60	10.23	4.05	1.71	9.47
Quartz bands in ore layer																						
WX28-8	1.39	2.79	0.35	1.22	0.25	0.05	0.15	0.02	0.15	0.03	0.08	0.02	0.14	0.02	6.63	0.71	0.94	3.10	6.84	3.51	0.89	10.01
WX28-9	5.70	11.78	1.36	4.83	0.98	0.20	0.74	0.09	0.70	0.11	0.50	0.10	0.75	0.12	27.96	0.72	0.99	2.26	5.16	3.68	0.81	7.92
Clay bands in ore layer																						
WX24-3	61.16	134.12	16.21	57.92	9.34	1.37	4.26	0.56	4.31	0.80	3.37	0.59	4.84	0.84	299.68	0.66	1.00	4.17	8.54	4.12	0.71	14.24
WX24-5	37.50	80.60	9.29	33.23	6.46	1.21	4.55	0.61	3.64	0.55	2.08	0.33	2.41	0.36	182.82	0.68	1.01	4.82	10.53	3.66	1.53	11.50
Fluid inclusions in quartz from banded ore																						
WX9-13	0.73	2.29	0.20		0.13	0.03	0.05	0.01	0.04	0.01	0.01	0.00	0.01	0.00	3.50	1.18	1.42	24.57	49.46	3.57	4.30	26.74
WX9-22	1.64	4.29	0.41	1.17	0.36	0.08	0.24	0.03	0.13	0.01	0.03	0.00	0.04	0.01	8.43	0.83	1.24	10.16	27.66	2.83	4.80	16.22
WX18-9	32.66	61.51	8.48	24.35	4.21	0.94	2.49	0.25	0.82	0.06	0.14	0.01	0.09	0.01	136.00	0.88	0.87	95.43	247.95	4.88	22.67	33.97

Chondrite-normalizing values from Taylor and McLennan (1985). $\sum$REE=$\sum$(La−Lu); Eu/Eu*=$(Eu)_n/((Sm)^*_n(Gd)_n)^{1/2}$, Ce/Ce*=$(Ce)_n/((La)^*_n(Pr)_n)^{1/2}$, $\sum$LREE/$\sum$HREE=$\sum$(La−Sm)/$\sum$(Gd−Lu) (McLennan, 1989).

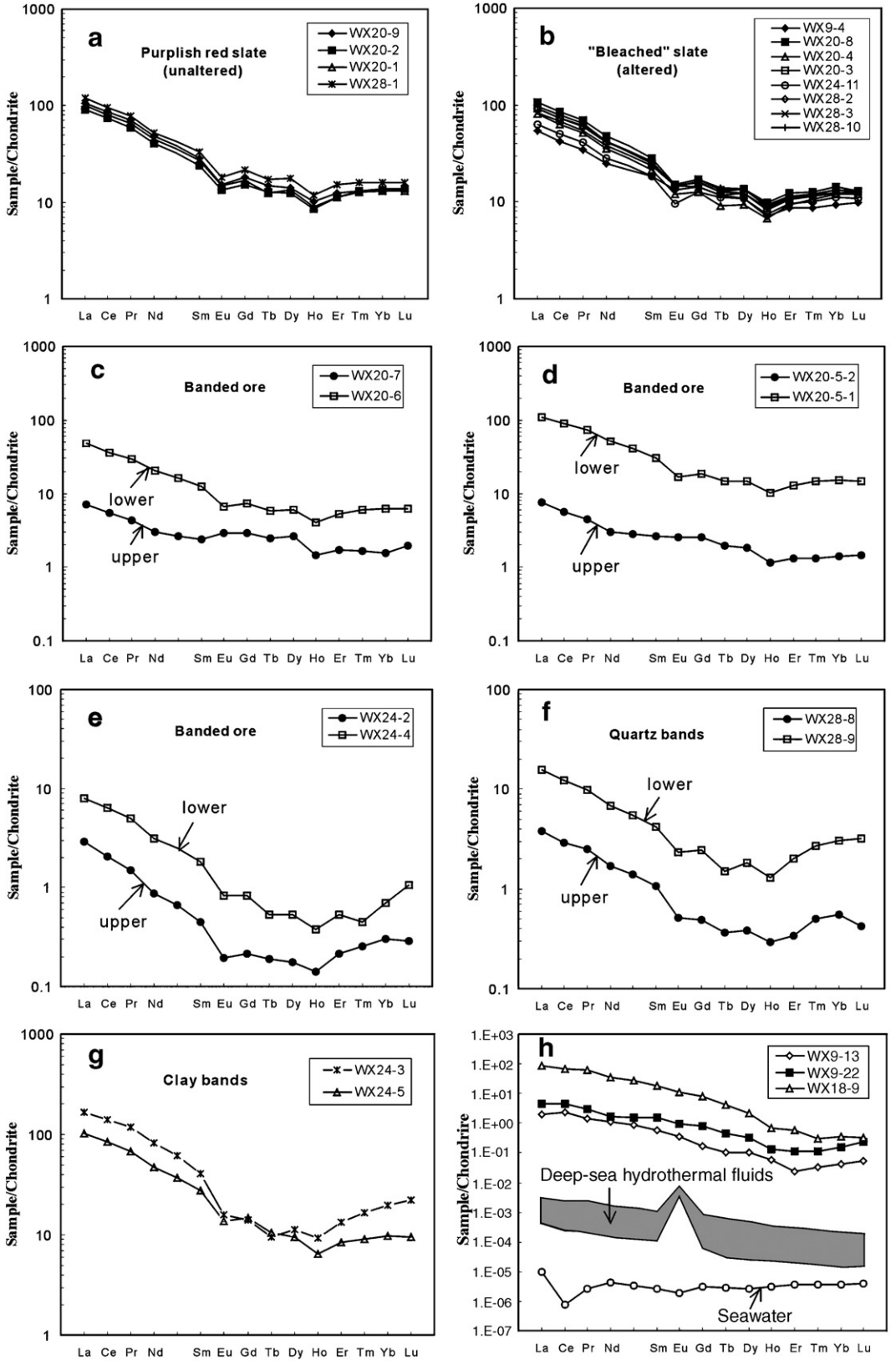
a
Purplish red slate (unaltered)
WX20-9
WX20-2
WX20-1
WX28-1
b
"Bleached" slate (altered)
WX9-4
WX20-8
WX20-4
WX20-3
WX24-11
WX28-2
WX28-3
WX28-10
c
Banded ore
WX20-7
WX20-6
lower
upper
d
Banded ore
WX20-5-2
WX20-5-1
lower
upper
e
Banded ore
WX24-2
WX24-4
lower
upper
f
Quartz bands
WX28-8
WX28-9
lower
upper
g
Clay bands
WX24-3
WX24-5
h
WX9-13
WX9-22
WX18-9
Deep-sea hydrothermal fluids
Seawater
Sample/Chondrite
Sample/Chondrire
La Ce Pr Nd Sm Eu Gd Tb Dy Ho Er Tm Yb Lu

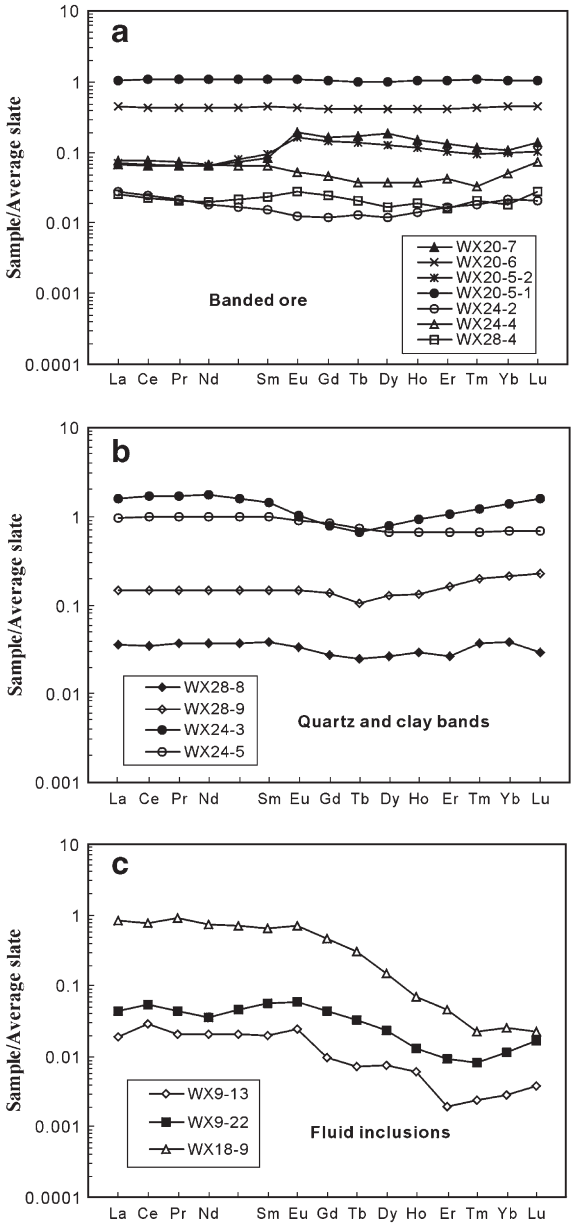

Fig. 6. Average unaltered slate-normalized REE patterns for banded ores (a), quartz and clay bands (b), and fluid inclusions in quartz (c).

Madiyi Formation, with a strike length of 40 to 350 m and a dip extent up to 3500 m (Figs. 1–3). The ores are characterized by rhythmic fine layering of stibnite, scheelite, pyrite, quartz, and metasediments (silty clays) on both the macro- and micro-scales (Fig. 4a, b, and f), as observed in many other sedimentary exhalative (sedex) ore deposits (e.g., Han and Hutchinson, 1989; Large et al., 1998; Paradis et al., 1998; Jiang et al., 1998, 1999; Emsbo et al., 1999; Gu et al., 2002c). In some cases, both the ore layers and, in detail, the microbands in the ore are folded along with their host metasedimentary rocks, suggesting that they predated regional metamorphism and were most probably coeval with deposition of the turbidites. In other places, structures of soft-sediment deformation due to slumping and synsedimentary sliding are observed in banded ores (Fig. 4e) and the barren quartz–carbonate beds (Fig. 4d) in the adjacent host rocks, where asymmetric and homoclinal, small-scale folds are bounded above and below by undisturbed beds.

Traceable over the distance of several to a few hundreds of m along bedding, stibnite, scheelite and Au-bearing quartz microbands or laminae of mm- to cm-scales are intricately interlayered with pelagic silty clay bands. The boundaries between different microbands are sharp and conformable on the microscale (Fig. 4f). Such sharp contacts would be difficult to maintain in a replacement scenario (Gu, 1996; Large et al., 1998). Chemical modeling by Cooke and Large (cf. Large et al., 1998) showed that more complicated, laterally zoned gangue assemblages should have formed if replacement was the principal mechanism. However, such zonations are absent in the Woxi ores.

Further evidence for a syngenetic origin of the Woxi deposit includes the relationship between stratiform ores and stringers as well as the distribution style of alteration. The stockwork mineralization at Woxi, characterized by numerous quartz+pyrite+gold+scheelite stringer veins and veinlets, lies immediately beneath the stratiform ore layers and is completely absent in the hanging wall (Figs. 3 and 4c), strongly suggesting that it most likely represents feeder zones in a sedimentary exhalative system. Since a focused, sustained discharge fault to the Woxi stratiform ores has not been identified, hydrothermal fluids were not channeled to specific discharge sites and must have migrated upward onto the basin floor through diffuse, fissure-related feeder stockworks within the soft sediment pile. Typical stringer veinlets in the deposit occur as 0.5 to 5 cm wide, crosscutting stockworks that exhibit open-space textures, indicating that the fluid pressure was likely close to, and intermittently exceeded, lithostatic pressure and that the hydraulic fracture-style

Fig. 5. Chondrite-normalized REE diagrams for unaltered and altered rocks (a–b), banded ores (c–e), quartz and clay bands (f–g) in banded ores, and fluid inclusions in quartz bands (h) from the Woxi deposit. REE distributions of hydrothermal fluids from the East Pacific Rise (Douville et al., 1999) and seawater (Elderfield and Greaves, 1982) are also shown on (h). Chondrite-normalizing values taken from Taylor and McLennan (1985).

stockworks developed in an extensional stress regime, close to the seawater–rock interface (Large, 1992).

At Woxi, alteration is more intense and generally thicker in the footwall than in the hanging wall (Figs. 3 and 4a). This is in contrast to the phenomenon observed in many epigenetic, hydrothermal replacement/infilling ore deposits where the hanging wall rocks are commonly more intensely and widely altered than the footwall rocks (e.g., Dubé et al., 1998; Sun et al., 2001), especially when ore veins were gentle and flat at the time of formation. We thus interpret the semiconformable, tabular alteration at Woxi to be cogenetic with mineralization. The hanging wall alteration blanket may represent the latest stage of hydrothermal activity after the system evolved into an ore-forming environment, whereas the footwall alteration may have formed before and during the main mineralizing event, or even after the mineralizing event as hydrothermal fluids continued to percolate through the unconsolidated sediment pile.

Restriction of stringers to the footwall stratigraphy and the generally more intense and widespread alteration zone in the footwall rocks than the hanging wall rocks are common features of both volcanogenic and sedimentary exhalative ore deposits (e.g., Gemmell and Large, 1992; Whitehead et al., 1996; Robinson et al., 1996; Sherlock et al., 1999; Doyle and Huston, 1999). We consider that a synsedimentary ore genesis model best explains the intimate spatial relationship between the stratiform ores, the stringers, and the alteration at Woxi described above. Synthesis of the stratigraphically repeated mineralized sequences in the deposit suggests that mineralization was episodic, accompanied and periodically interrupted by turbiditic sedimentation. Each exhalative episode was preceded by a period of mixing, both chemical and turbiditic sedimentation (footwall alteration blanket), followed by a peak release of hot metalliferous brines (stratiform ores and associated stringers), and terminated by a waning influx of hydrothermal fluids accompanying turbiditic deposition (hanging wall alteration blanket).

6.2. Genetic implications of REE geochemistry

Previous studies have demonstrated that REE signatures of clastic and chemical metasediments are mainly controlled by their provenance and that, in the absence of partial melting and intense metasomatism involving large fluid volumes and high fluid/rock ratios, pre-existing REE signatures remained unaffected by diagenetic or metamorphic processes (e.g., Taylor and McLennan, 1985; Taylor et al., 1986; Lottermoser, 1989a,b; Bau, 1991; Lottermoser, 1992; Parr, 1992; Siva Siddaiah et al., 1994; Bierlein, 1995). Both unaltered and altered metasediments in this study display REE patterns very similar to upper continental crust and typical post-Archean shales (Taylor and McLennan, 1985), suggesting extremely low REE mobilization and preservation of primary REE signatures during post-depositional processes. Thus, the REE geochemistry of these metasedimentary rocks and associated ore deposits may provide important constraints for interpretation of ore genesis.

An increasing number of studies on fluids from various deep-sea hydrothermal systems have demonstrated that the chondrite-normalized REE patterns of acidic hydrothermal fluids exhibit LREE-enriched profiles with strikingly positive Eu anomalies (Eu/Eu∗ up to 30; Michard et al., 1983; Michard and Albarède, 1986; Campbell et al., 1988; Michard, 1989; Fouquet et al., 1993; Klinkhammer et al., 1994; Mitra et al., 1994; James et al., 1995; Bau and Dulski, 1999; Douville et al., 1999). Compared to the modern deep-sea hydrothermal fluids, the fluids responsible for the formation of stratiform ores at Woxi possess variable but distinctly higher total REE contents (3.5 to 136 ppm), approximately 3 to 5 orders of magnitude greater than the former (ppb levels). With the exception of non- or insignificant Eu anomalies, however, their chondrite-normalized REE patterns are overall comparable with those of the oceanic hydrothermal fluids (Fig. 5h). Klinkhammer et al. (1994) showed that the principal process fixing the REE-pattern of deep-sea hydrothermal fluids from mid-ocean ridges is ion exchange with hydrothermal plagioclases during dissolution and recrystallization of MORB plagioclase, which generally has a large positive Eu anomaly. Since the dominant rocks available for the circulating fluid system at Woxi are silicate-rich turbidites deposited in a continental back arc basin and plagioclase constitutes less than 5% of the rocks (Gu et al., 2002a,b), the lack of characteristic positive Eu anomalies for the Woxi fluids is not surprising.

Wide variations in total REE concentrations of hydrothermal fluids, such as those present in this study, are also observed in different hydrothermal fields from mid-ocean ridges. Klinkhammer et al. (1994) reported that while there is a broad similarity in the shape of fluid patterns from different environments, there exist wide variations in REE concentrations (up to 2 orders of magnitude), even between vents in the same field and at the same vent with time. In general, REE concentrations of hydrothermal solutions are controlled by: (a) REE contents of source rocks; (b) physicochemical parameters of the solution, such as temperature, pH, and concentrations of ligands available for

REE complexation; and (c) fluid/rock volume ratios and duration of fluid–rock interaction. Michard (1989) analyzed hydrothermal fluids from a variety of geological environments and found that the total REE concentrations increase with decreasing pH, independent of rock type and temperature. For instance, REE concentrations in a hydrothermal fluid from the Valles Caldera, New Mexico, with an acidic pH (~2.5) are 3 orders of magnitude greater than those in a neutral (pH=7.1) hydrothermal fluid in the same geothermal area (Michard, 1989). In addition, REE concentrations tend to be higher where temperatures are higher and water/rock ratios are lower (Van Middlesworth and Wood, 1998).

The ore-bearing solutions at Woxi have significantly higher total REE concentrations (ppm levels) than the modern hydrothermal fluids (ppb levels). Fluid inclusion studies conducted on banded quartz and scheelite at Woxi showed that the homogenization temperatures range between 100 and 260 °C (typically <200 °C) and the salinities vary from 3 to 9 wt.% NaCl equiv. (Liu et al., 1993; Luo et al., 1996; Gu et al., 2002a). Thermodynamic calculations based on fluid inclusion analyses indicated near-neutral to alkaline (pH=6.4 to 8.1) and mildly reducing ($\log f_{O_2}=-36$ to -42) fluid compositions (Liu et al., 1993). Therefore, it rules out high temperature and strongly acidic fluid compositions in the Woxi deposit. Although the formation of metal ligand complexes may greatly enhance the stability of the REE in hydrothermal fluids and, in some cases, unusually high concentrations of strong ligands such as CO_3^{2-}, SO_4^{2-} or F^- might induce REE mobility under less severe pH and low temperature conditions (Wood, 1990a,b; Ménager et al., 1992; Haas et al., 1995; Gammons et al., 1996), it is unlikely that complexation by anions in the circulating fluids was responsible for drawing REE in the Woxi solution. In typical low to moderate temperature, near-neutral to alkaline and mildly reducing solutions, such as those present in the Woxi deposit, CO_3^{2-} and/or SO_4^{2-} should be the dominant complexing agents and preferential mobilization of HREE (HREE-enriched but not LREE-enriched) would be expected (Brookins, 1989; Wood, 1990b; Bau, 1991; Klinkhammer et al., 1994; Bierlein, 1995; Douville et al., 1999). However, this is clearly not the case (Fig. 5h). In addition, even in seawater with chloride as prevalent anion, the chloride complexes are insignificant in the pH range of 5 and above (Brookins, 1989). Therefore, it is reasonable to speculate that the significantly high REE concentrations of the Woxi fluids may have resulted from the mobilization of these elements in the source rocks, relatively low fluid/rock ratios, and/or perhaps circulating over extremely long periods of time. Similarly high REE concentrations of fluid inclusions in quartz were also documented in the Lannigou and Yata Carlin-type gold deposits (3 to 84 ppm; Su et al., 1998) in SW-Guizhou and the Kuroko-type Gacun Ag-polymetallic ore deposit (5–149 ppm; Bie et al., 2000) in Sichuan, China.

In summary, the REE geochemistry is consistent with the syngenetic (sedex) model, in which the original hydrothermal fluids responsible for the formation of the Woxi W–Sb–Au deposit were derived from evolved seawater that circulated through the sediment pile and subsequently exhaled on the seafloor. Compared to recent metalliferous fluids from various deep-sea hydrothermal fluids, the ore fluids at Woxi are depleted in Eu due to lack of feldspar (plagioclase) in the source rocks available for the circulating fluids. The high REE concentrations of the fluids reflect the net result of several processes, including reactions with REE-rich source rocks, leaching within a relatively low fluid/rock system, and even circulating over extremely long periods of time.

The partitioning behavior of REE between aqueous solutions and precipitating minerals for conditions appropriate to hydrothermal systems is still not well understood due to the fact that partitioning experiments on REE have largely been concerned with magmatic systems at high temperatures and high pressures (e.g., Cullers et al., 1973; Flynn and Burnham, 1978; Wendlandt and Harrison, 1979). Thus, the amount of REE fractionation which occurs during precipitation of hydrothermal minerals is often difficult to assess but may affect only Eu and the LREE/HREE ratios (Cullers and Graf, 1984).

Pure submarine chemical precipitates (exhalites) from various modern hydrothermally active areas, e.g., the Red Sea (Courtois and Treuil, 1977), the East Pacific Rise (EPR; Alt, 1988; German et al., 1999) and the Mid-Atlantic Ridge (MAR; Mills and Elderfield, 1995b) commonly inherit REE patterns of their parent hydrothermal fluids, with a pronounced LREE enrichment and distinct positive Eu anomalies. Such patterns, however, could be modified depending on the degree of mixing with seawater, the length of exposure time to the seawater and the degree of subaqueous oxidation (Bonatti et al., 1976; Marchig et al., 1986; Lottermoser, 1992). In contrast, hydrogenous metalliferous Fe–Mn sediments precipitated on the sea floor have REE distributions very similar to that of seawater (typically LREE-, Ce-, Eu-depleted and HREE-enriched; e.g., Bender et al., 1971; Piper and Graef, 1974; Robertson and Fleet, 1976; Dymond et al., 1977; Marchig et al., 1986; Colley and Walsh, 1987), indicating a seawater

source for the REE (Lottermoser, 1992). Lottermoser (1989a) and Parr (1992) documented systematic changes in the REE signatures of a variety of exhalites associated with Broken Hill-type mineralization and concluded that the REE profiles in these chemical sediments reflect physico-chemical conditions of the exhalative fluids from which they precipitated. Exhalites proximal to sulphide deposits possess LREE enrichment and positive Eu anomalies, similar to REE patterns of pure chemical sediments and hydrothermal fluids of the East Pacific Rise. By contrast, exhalites in distal position from Broken Hill-type mineralization exhibit similar LREE enrichments, but have negative Eu anomalies, suggesting decreasing temperatures, fO_2 changes and mixing of the hydrothermal fluids with seawater, in addition to an increasing clastic component during deposition of the exhalative precipitates.

Compared to the ore-forming fluids, the bulk stratiform ores at Woxi are markedly enriched in HREE (lower Nd_N/Yb_N, La_N/Yb_N and ∑LREE/∑HREE; Table 1), with similar or slightly more pronounced negative Eu anomalies (Eu/Eu*=0.63 to 1.14; Table 1 and Fig. 7a). Enrichment in HREE and depletion in Eu of hydrothermal sediments relative to their parent fluids were also observed at the MAR (Mills and Elderfield, 1995b) and the EPR (Alt, 1988; German et al., 1999). They are commonly attributed either to crystallographic controlling on REE fractionation between chemical sediments and parent fluids during precipitation (Guichard et al., 1979; Morgan and Wandless, 1980; Alt, 1988; Mills and Elderfield, 1995b) or to seawater influence (German et al., 1990; Mills and Elderfield, 1995b; German et al., 1997, 1999). While the HREE enrichment and Eu depletion of the white smoker chimney sulphide with respect to the parent fluid at the TAG Mound, MAR are thought to be due to preferential substitution of the smaller HREE into the sulphide lattice, the HREE-enriched and Eu-depleted patterns of the chimney oxides relative to parent fluid are interpreted to reflect various mixtures of seawater and hydrothermal fluid (Mills and Elderfield, 1995b). Recent study on a hydrothermal sediment core from the OBS vent-field, EPR (German et al., 1999) showed that the hydrothermal sediments have much smaller positive Eu-anomalies than the parent vent fluid and the REE patterns become flatter (more HREE-enriched) up-core, indicating an increasing seawater influence.

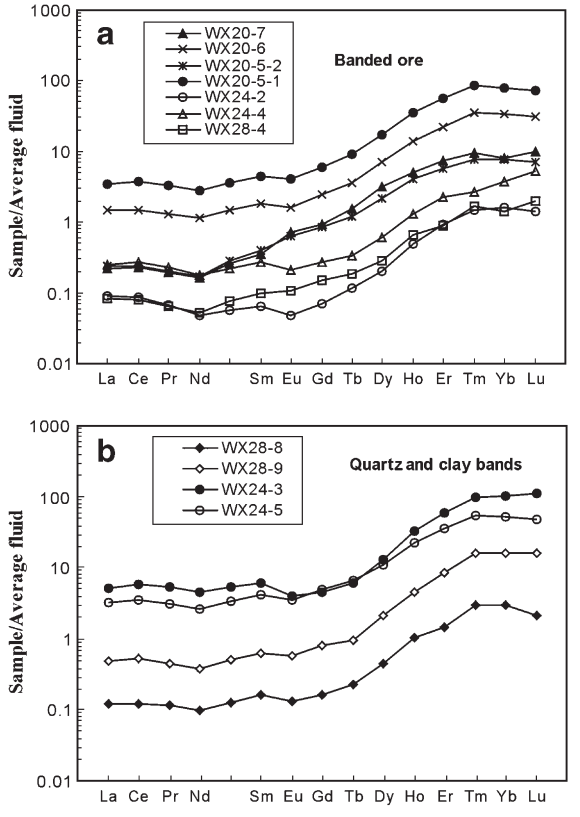

Fig. 7. Average fluid-normalized REE patterns for banded ores (a) and quartz and clay bands (b).

As the bulk stratiform ores at Woxi exhibit REE patterns very similar to individual quartz bands within the ore (Figs. 5–7), indicating a mineral proportion-independent nature of the REE distributions, and since we know that sulphide REE concentrations are commonly too low to contribute substantially to the REE pattern of the ores (Mills and Elderfield, 1995b), we are left with the idea that the characteristic HREE enrichment and Eu depletion of the Woxi ores relative to the parent fluid are related to crystallographic control. We thus interpret the observed patterns to reflect the influence of adsorptive scavenging of REE from seawater. This conclusion is in agreement with the variation of REE distributions observed within a single ore layer. The degree of HREE enrichment tends to increase (Nd_N/Yb_N, La_N/Yb_N and ∑LREE/∑HREE ratios decrease) up-layer while the total REE concentrations decrease (Fig. 5c–e; Table 1), suggesting a more significant influence and more advanced dilution by seawater with time. However, the ore samples show no negative Ce anomalies. This may imply that the hydrothermal fluid was not oxidized enough by seawater to allow the oxidation of Ce to the tetravalent state.

A comparison of the Woxi ore REE patterns with exhalites from the sedex-type Dachang Sn-polymetallic ore deposit and from the Sullivan Pb–Zn deposit is

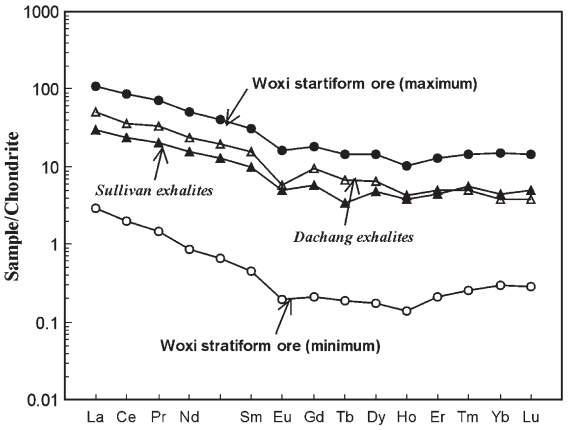

Fig. 8. Comparison of chondrite-normalized REE patterns of the stratiform ores at Woxi with the typical exhalites from the Sullivan Pb–Zn deposit and the Dachang Sn-polymetallic ore deposit (Han and Hutchinson, 1989).

shown in Fig. 8. Exhalites, including banded to laminated tourmalinites, sulphide-rich siliceous rocks and K-feldspar-rich rocks from the Dachang Sn-polymetallic ore deposit possess moderate but variable REE concentrations on the order of 31 to 111 ppm. The average chondrite-normalized REE pattern is very similar to the Woxi banded to laminated quartz–stibnite–scheelite ores, with comparable LREE enrichment (La_N/Yb_N=6.2 to 18.5, ∑LREE/∑HREE=5 to 14) and negative Eu anomalies (Eu/Eu*=0.20 to 0.68; Han and Hutchinson, 1989). A banded tourmaline-rich exhalite from the Sullivan deposit has total REE concentrations of 58 ppm and is similarly depleted in HREE (La_N/Yb_N=6.9, ∑LREE/∑HREE=7.6) and Eu (Eu/Eu*=0.66; Han and Hutchinson, 1989). Such broad similarities in both the shape of chondrite-normalized patterns and the amount of REE fractionation among the ores and exhalites from different ore deposits simply suggest a similar genesis for the formation of these deposits.

7. Conclusions

The REE signatures of the metasedimentary rocks and associated ores from the Woxi W–Sb–Au deposit remained unchanged during post-depositional processes and were mainly controlled by their provenance. The original ore-forming hydrothermal fluids, characterized by variable and high total REE concentrations, marked LREE enrichment and no significant Eu-anomalies, were derived from evolved seawater that circulated through the clastic sedimentary pile and subsequently discharged on the seafloor.

The bulk ores are enriched in HREE and slightly depleted in Eu relative to their parent fluids, as observed in some deep-sea hydrothermal systems. This is interpreted as indicating the influence of seawater rather than the crystallographic control. Within a single ore layer the degree of HREE enrichment tends to increase upward, whereas the total REE concentration decreases, reflecting more significant influence and more advanced dilution of seawater with time.

There is a broad similarity in both the shape of chondrite-normalized REE patterns and the amount of REE fractionation between the ores in this study and the exhalites from other sedex-type polymetallic ore deposits, suggesting a similar genesis for the formation of these deposits. This conclusion is in agreement with geologic evidence supporting a syngenetic model for the Woxi deposit (Schulz et al., 2002; Gu et al., 2002a, 2003).

Acknowledgements

We are grateful to B.G. Pen, K.R. Zhang, M.B. Lei, L.J. Luo, Y.H. Gao, Z.G. Liu, K.Y. Liu, W.P. Chen, R.S. Yang, S.Y., Liu, J.H., Liang, and Z.B. Chen from the Woxi Gold Mine for their support during the field work. Critical reviews by Dr. P. J. McGoldrick and two anonymous reviewers have greatly improved the manuscript. We also acknowledge the insightful handling from Drs. S. G. Peters, Khin Zaw, H. Forster, T. Horscroft and N.J. Cook. The research was funded by the National Natural Science Foundation of China (NSFC, 40573031), the Scientific Research Foundation of Austria (FWF, P12026-GEO), and the 973 National Basic Research Priorities Program (2006CB701402). The first author is also supported by a special grant from the Chinese Academy of Sciences.

References

Alt, J.C., 1988. The chemistry and sulphur isotope composition of massive sulfide and associated deposits on Green Seamount, Eastern Pacific. Economic Geology 83, 1026–1033.

Balaram, V., Anjaiah, K.V., Reddy, M.R.P., 1995. Comparative study on the trace and rare earth element analysis of an Indian polymetallic nodule reference sample by inductively coupled plasma atomic emission spectrometry and inductively coupled plasma mass spectrometry. Analyst 120, 1401–1406.

Bau, M., 1991. Rare-earth element mobility during hydrothermal and metamorphic fluid–rock interaction and the significance of the oxidation state of europium. Chemical Geology 93, 219–230.

Bau, M., Dulski, P., 1999. Comparing yttrium and rare earths in hydrothermal fluids from the Mid-Atlantic Ridge: implications for Y and REE behaviour during near-vent mixing and for the Y/Ho ratio of Proterozoic seawater. Chemical Geology 155, 77–90.

Bender, M., Broecker, W., Gornitz, V., Middel, U., Kay, R., Sun, S.S., Biscaye, P., 1971. Geochemistry of three cores from the East Pacific Rise. Earth and Planetary Science Letters 12, 425–433.

Bhatia, M.R., 1985. Rare earth element geochemistry of Australian Paleozoic graywackes and mudrocks: provenance and tectonic control. Sedimentary Geology 45, 97–113.

Bie, F.L., Hou, Z.Q., Li, S.R., Su, W.C., Xu, J.H., 2000. Composition characteristics of rare earth elements in metallogenic fluid of the Gacun superlarge Kuroko-type deposit. Acta Petrologica Sinica 16 (4), 575–580 (in Chinese with English abstract).

Bierlein, F.P., 1995. Rare-earth element geochemistry of clastic and chemical metasedimentary rocks associated with hydrothermal sulphide mineralisation in the Olary Block, South Australia. Chemical Geology 122, 77–98.

Bonatti, E., Honnorez-Guerstein, M.B., Honnorez, J., Stern, C., 1976. Hydrothermal pyrite concretions from the Romanche Trench (equatorial Atlantic): metallogenesis in oceanic fracture zones. Earth and Planetary Science Letters 32, 1–10.

Brookins, D.G., 1989. Aqueous geochemistry of rare earth elements. In: Lipin, B.R., McKay, G.A. (Eds.), Geochemistry and Mineralogy of Rare Earth Elements. Reviews in Mineralogy, vol. 21. Mineralogical Society of America, pp. 210–225.

Campbell, A.C., Palmer, M.R., Klinkhammer, G.P., Bowers, T.S., Edmond, J.M., Lawrence, J.R., Casey, J.F., Thompson, G., Humphris, S., Rona, P., Karson, J.A., 1988. Chemistry of hot springs on the Mid-Atlantic Ridge. Nature 335, 514–519.

Chen, J., Jahn, B.-M., 1998. Crustal evolution of southeastern China: Nd and Sr isotopic evidence. Tectonophysics 284, 101–133.

Colley, H., Walsh, J.N., 1987. Genesis of Fe–Mn deposits of southwest Viti Levu, Fiji. Transactions, Institution of Mining and Metallurgy (Section B, Applied Earth Science) 96, 201–212.

Courtois, C., Treuil, M., 1977. Distribution des terres rares et de quelques éléments en trace dans les sédiments récents des fosses de la Mer Rouge. Chemical Geology 20, 57–72.

Cullers, R.L., Graf, J.L., 1984. Rare earth elements in igneous rocks of the continental crust: intermediate and silicic rocks–ore petrogenesis. In: Henderson, P. (Ed.), Developments in Geochemistry, vol. 2. Rare Earth Element Geochemistry. Elsevier, Amsterdam, pp. 275–316.

Cullers, R.L., Medaris, L.G., Haskin, L.A., 1973. Experimental studies of the distribution of rare earths as trace elements among silicate minerals and liquids and water. Geochimica et Cosmochimica Acta 37, 1499–1512.

Davies, J.F., Prevec, S.A., Whitehead, R.E., Jackson, S.E., 1998. Variations in REE and Sr-isotope chemistry of carbonate gangue, Castellanos Zn–Pb deposit, Cuba. Chemical Geology 144, 99–119.

Douville, E., Bienvenu, P., Charlou, J.L., Fouquet, Y., Appriou, P., Gamo, T., 1999. Yttrium and rare earth elements in fluids from various deep-sea hydrothermal systems. Geochimica et Cosmochimica Acta 63, 627–643.

Doyle, M.G., Huston, D.L., 1999. The subsea-floor replacement origin of the Ordovician Highway-Reward volcanic-associated massive sulfide deposit, Mount Windsor Subprovince, Australia. Economic Geology 94, 825–844.

Dubé, B., Dunning, G., Lauzière, K., 1998. Geology of the Hope Brook Mine, Newfoundland, Canada: a preserved late Proterozoic high-sulfidation epithermal gold deposit and its implications for exploration. Economic Geology 93, 405–436.

Dymond, J., Corliss, J.B., Heath, G.R., 1977. History of metalliferous sedimentation at Deep Sea Drilling site 319 in the South Eastern Pacific. Geochimica et Cosmochimica Acta 41, 741–753.

Elderfield, H., Greaves, M.J., 1982. The rare earth elements in seawater. Nature 296, 214–219.

Emsbo, P., Hutchinson, R.W., Hofstra, A.H., Volk, J.A., Bettles, K.H., Baschuk, G.J., Johnson, C.A., 1999. Syngenetic Au on the Carlin trend: implications for Carlin type deposits. Geology 27, 59–62.

Flynn, R.T., Burnham, C.W., 1978. An experimental determination of rare earth partition coefficients between a chloride containing vapor phase and silicate melts. Geochimica et Cosmochimica Acta 42, 685–701.

Fouquet, Y., von Stackelberg, U., Charlou, J.C., Erzinger, J., Herzig, P.M., Muehe, R., Wiedicke, M., 1993. Metallogenesis in back-arc environments: the Lau basin example. Economic Geology 88, 2154–2181.

Gammons, C.H., Wood, S.A., Williams-Jones, A.E., 1996. The aqueous geochemistry of the rare earth elements and Y: VI. Stability of neodymium chloride complexes from 25 to 300 °C. Geochimica et Cosmochimica Acta 60, 4615–4630.

Gemmell, J.B., Large, R.R., 1992. Stringer system and alteration zones underlying the Hellyer volcanic-hosted massive sulfide deposit, Tasmania, Australia. Economic Geology 87, 620–649.

German, C.R., Klinkhammer, G.P., Edmond, J.M., Mitra, A., Elderfield, H., 1990. Hydrothermal scavenging of rare earth elements in the ocean. Nature 345, 516–518.

German, C.R., Ludford, E.M., Palmer, M.R., O'Brien, J.D., Patching, J.W., Floch'lay, G., Appriou, P., Barriga, F., Miranda, M., Fouquet, Y., Bougault, H., 1997. Hydrothermal plumes on the Mid-Atlantic Ridge (Azores): particle geochemistry and mineralogy—MARFLUX/ATJ. Terra Nova 9, 539.

German, C.R., Hergt, J., Palmer, M.R., Edmond, J.M., 1999. Geochemistry of a hydrothermal sediment core from the OBS vent-field, 21°N East Pacific Rise. Chemical Geology 155, 65–75.

Ghazi, A.M., Vanko, D.A., Roedder, E., Seeley, R.C., 1993. Determination of rare earth elements in fluid inclusions by inductively coupled plasma–mass spectrometry (ICP–MS). Geochimica et Cosmochimica Acta 57, 4513–4516.

Grauch, R.I., 1989. Rare earth elements in metamorphic rocks. In: Lipin, B.R., McKay, G.A. (Eds.), Geochemistry and Mineralogy of Rare Earth Elements. Reviews in Mineralogy, vol. 21. Mineralogical Society of America, pp. 147–167.

Gromet, L.P., Dymek, R.F., Haskin, L.A., Korotev, R.L., 1984. The North American Shale Composite: its composition, major and trace element characteristics. Geochimica et Cosmochimica Acta 48, 2469–2482.

Gu, X.X., 1994. Geochemical characteristics of the Triassic Tethys-turbidites in the northwestern Sichuan, China: implications for provenance and interpretation of the tectonic setting. Geochimica et Cosmochimica Acta 58, 4615–4631.

Gu, X.X., 1996. Turbidite-Hosted Micro-Disseminated Gold Deposits. Chengdu University of Science and Technology Press, Chengdu. 239 pp.

Gu, X.X., Schultz, O., Vavtar, F., Liu, J.M., Zheng, M.H., 2002a. Jungproterozoische submarine Primäranreicherung und metamorphogene Weiterentwicklung der stratiformen W–Sb–Au–Erzlagerstätten vom "Typ Woxi" in Hunan (Süd-China). Archiv für Lagerstätte Forschung, Geologisches Bundesamt, vol. 23. Vienna, 204 pp.

Gu, X.X., Liu, J.M., Zheng, M.H., Tang, J.X., Qi, L., 2002b. Provenance and tectonic setting of the Proterozoic turbidites in Hunan, South China: geochemical evidence. Journal of Sedimentary Research 72, 393–407.

Gu, X.X., Liu, J.M., Schulz, O., Vavtar, F., Zheng, M.H., 2002c. Syngenetic origin for the sediment-hosted disseminated gold

deposits in NW-Sichuan, China: ore fabric evidence. Ore Geology Reviews 22, 91–116.

Gu, X.X., Schulz, O., Vavtar, F., Liu, J.M., Zheng, M.H., 2003. Ore fabric characteristics and their genetic significance of the Woxi W–Sb–Au deposit, Hunan. Mineral Deposits 22, 107–120 (in Chinese with English abstract).

Gu, X.X., Liu, J.M., Schulz, O., Vavtar, F., Zheng, M.H., 2004. Syngenetic origin for the Woxi W-Sb-Au deposit in human: evidence from trace elements and sulfur isotopes. Chinese Journal of Geology 39 (3), 424–439 (in Chinese with English abstract).

Guichard, F., Church, T.M., Treuil, M., Jaffrezic, H., 1979. Rare earths in barites: distribution and effects on aqueous partitioning. Geochimica et Cosmochimica Acta 43, 983–997.

Haas, J.R., Shock, E.L., Sassini, D.C., 1995. Rare earth elements in hydrothermal systems: estimates of standard partial modal thermodynamic properties of aqueous complexes of the rare earth elements at high pressures and temperatures. Geochimica et Cosmochimica Acta 59, 4329–4350.

Han, F., Hutchinson, R.W., 1989. Evidence for the exhalative hydrothermal sedimentary origin of the Dachang Sn-polymetallic deposit – trace element and rare earth element geochemistry of the host rocks. Mineral Deposits 8 (3), 33–44 (in Chinese with English abstract).

Haskin, L.A., 1984. Petrogenetic modelling – use of rare earth elements. In: Henderson, P. (Ed.), Rare Earth Element Geochemistry. Developments in Geochemistry, vol. 2. Elsevier, Amsterdam, pp. 115–152.

James, R.H., Elderfield, H., Palmer, M.R., 1995. The chemistry of hydrothermal fluids from the Broken Spur site, 29N Mid-Atlantic Ridge. Geochimica et Cosmochimica Acta 59, 651–659.

Jiang, S.Y., Palmer, M.R., Slack, J.F., Shaw, D.R., 1998. Paragenesis and chemistry of multistage tourmaline formation in the Sullivan Pb–Zn–Ag deposit, British Columbia. Economic Geology 93, 47–67.

Jiang, S.Y., Han, F., Shen, J.Z., Palmer, M.R., 1999. Chemical and Rb–Sr, Sm–Nd isotopic systematics of tourmaline from the Dachang Sn-polymetallic ore deposit, Guangxi Province, P.R. China. Chemical Geology 157, 49–67.

Klinkhammer, G.P., Elderfield, H., Edmond, J.M., Mitra, A., 1994. Geochemical implications of rare earth element patterns in hydrothermal fluids from mid-ocean ridges. Geochimica et Cosmochimica Acta 58, 5105–5113.

Large, R.R., 1992. Australian volcanic-hosted massive sulfide deposits: features, styles, and genetic models. Economic Geology 87, 471–510.

Large, R.R., Bull, S.W., Cooke, D.R., McGoldrick, P.J., 1998. A genetic model for the HYC deposit, Australia: based on regional sedimentology, geochemistry, and sulfide–sediment relationship. Economic Geology 93, 1345–1368.

Li, Z.X., Zhang, L., Powell, C.Mc.A., 1995. South China in Rodinia: part of the missing link between Australia–East Antarctica and Laurentia? Geology 23, 407–410.

Liu, Y.J., Sun, C.Y., Ma, D.S., 1993. Jiangnan-Type Gold Deposits and their Ore-Forming Geochemical Background. Nanjing University Press, Nanjing. 260 pp. (in Chinese).

Lottermoser, B.G., 1989a. Rare earth element study of exhalites within the Willyama Supergroup, Broken Hill Block, Australia. Mineralium Deposita 24, 92–99.

Lottermoser, B.G., 1989b. Rare-earth element behaviour associated with stratabound scheelite mineralisation (Broken Hill, Austria). Chemical Geology 78, 119–134.

Lottermoser, B.G., 1992. Rare earth elements and hydrothermal ore formation processes. Ore Geology Reviews 7, 25–41.

Luo, X.L., 1990. On source of ore-forming materials of Precambrian Au deposits, Hunan Province. Journal of the Guilin College of Metallogeny and Geology 10, 13–26 (in Chinese with English abstract).

Luo, X.L., 1994. Geological characteristics of Precambrian antimony metallogeny in Hunan. Journal of the Guilin College of Metallogeny and Geology 14, 335–349 (in Chinese with English abstract).

Luo, X.L., Yi, S.J., Liang, J.C., 1984. On the genesis of the Woxi Au–Sb–W deposit, W-Hunan. Geological Exploration for Non-ferrous Metals 20 (7), 1–10 (in Chinese).

Luo, X.L., Zhong, D.Q., Li, G.S., 1996. Geology of the Woxi-type Stratabound Gold Deposits in Hunan Province. Seismic Press, Beijing. 313 pp. (in Chinese with English abstract).

Ma, D.S., 1991. Geochemistry and genesis of the Proterozoic stratabound gold deposits in Jiangnan. Bulletin of Nanjing University (Natural Sciences) 4, 753–764 (in Chinese with English abstract).

Ma, D.S., Liu, Y.J., 1992. Geochemical characteristics and genesis of stratabound gold deposits in Jiangnan gold metallogenic belt. Science in China. Series B, Chemistry, Life Sciences & Earth Sciences 35, 240–256 (in Chinese with English abstr.).

Marchig, V., Erzinger, J., Heinze, P.M., 1986. Sediment in the black smoker area of the East Pacific Rise (18.5°S). Earth and Planetary Science Letters 79, 93–106.

McKay, G.A., 1989. Partitioning of rare earth elements between major silicate minerals and basaltic melts. In: Lipin, B.R., McKay, G.A. (Eds.), Geochemistry and Mineralogy of Rare Earth Elements. Reviews in Mineralogy, vol. 21. Mineralogical Society of America, pp. 45–74.

McLennan, S.M., 1989. Rare earth elements in sedimentary rocks: influence of provenance and sedimentary processes. In: Lipin, B. R., McKay, G.A. (Eds.), Geochemistry and Mineralogy of Rare Earth Elements. Reviews in Mineralogy, vol. 21. Mineralogical Society of America, pp. 169–200.

McLennan, S.M., Taylor, S.R., McCulloch, M.T., Maynard, J.B., 1990. Geochemical and Nd–Sr isotopic composition of deep-sea turbidites: crustal evolution and plate tectonic associations. Geochimica et Cosmochimica Acta 54, 2015–2050.

McLennan, S.M., Hemming, S., McDaniel, D.K., Hanson, G.N., 1993. Geochemical approaches to sedimentation, provenance, and tectonics. Geological Society of America, Special Paper 284, 21–40.

McLennan, S.M., Hemming, S.R., Taylor, S.R., Eriksson, K.A., 1995. Early Proterozoic crustal evolution: geochemical and Nd–Pb isotopic evidence from metasedimentary rocks, southwestern North America. Geochimica et Cosmochimica Acta 59, 1153–1177.

Ménager, M.-T., Menet, C., Petit, J.-C., Cathelineau, M., Come, B., 1992. Dispersion of U, Th and REE by water–rock interaction around an intergranitic U-vein, Jalerys Mine, Morvan, France. Applied Geochemistry, Supplement 1, 239–252.

Michard, A., 1989. Rare earth element systematics in hydrothermal fluids. Geochimica et Cosmochimica Acta 53, 745–750.

Michard, A., Albarède, F., 1986. The REE content of some hydrothermal fluids. Chemical Geology 55, 51–60.

Michard, A., Albarède, F., Michard, G., Minster, J.-F., Charlou, J.L., 1983. Rare-earth elements and uranium in high-temperature

solutions from East Pacific Rise hydrothermal vent field (13°N). Nature 303, 795–797.

Mills, R.A., Elderfield, H., 1995a. Hydrothermal activity and the geochemistry of metalliferous sediment. Geophysical Monograph 91, 392–407 (AUG).

Mills, R.A., Elderfield, H., 1995b. Rare earth element geochemistry of hydrothermal deposits from the active TAG Mound, 26°N Mid-Atlantic Ridge. Geochimica et Cosmochimica Acta 59, 3511–3524.

Mitra, A., Elderfield, H., Greaves, M.J., 1994. Rare earth elements in submarine hydrothermal fluids and plumes from the Mid-Atlantic Ridge. Marine Chemistry 46, 217–235.

Morgan, J.W., Wandless, G.A., 1980. Rare earth element distribution in some hydrothermal minerals: evidence for crystallographic control. Geochimica et Cosmochimica Acta 44, 973–980.

Paradis, S., Nelson, J.L., Irwin, S.E.B., 1998. Age constraints on the Devonian shale-hosted Zn–Pb–Ba deposits, Gataga district, Northeastern British Columbia, Canada. Economic Geology 93, 184–200.

Parr, J.M., 1992. Rare-earth element distribution in exhalites associated with Broken Hill-type mineralisation at the Pinnacles deposit, New South Wales, Australia. Chemical Geology 100, 73–91.

Piper, D.Z., Graef, P.A., 1974. Gold and rare-earth elements in sediments from the East Pacific Rise. Marine Geology 17, 287–297.

Robertson, A.H.F., Fleet, A.J., 1976. The origins of rare earths in metalliferous sediments of the Troodos Massif, Cyprus. Earth and Planetary Science Letters 28, 385–394.

Robinson, M., Godwin, C.I., Stanley, C.R., 1996. Geology, lithogeochemistry, and alteration of the Battle volcanogenic massive sulfide zone, Buttle Lake Mining Camp, Vancouver Island, British Columbia. Economic Geology 91, 527–548.

Savelli, C., Marani, M., Gamberi, F., 1999. Geochemistry of metalliferous, hydrothermal deposits in the Aeolian arc (Tyrrhenian Sea). Journal of Volcanology and Geothermal Research 88, 305–323.

Schulz, O., Vavtar, F., Gu, X.X., 2002. Stratiforme Sb–W–Au–Lagerstätte Woxi in Hunan, China. Erzmetall 55, 535–540.

Sherlock, R.L., Roth, T., Spooner, E.T.C., Bray, C.J., 1999. Origin of the Eskay Creek precious metal-rich volcanogenic massive sulfide deposit: fluid inclusion and stable isotope evidence. Economic Geology 94, 803–824.

Sherrell, R.P., Field, M.P., Ravizza, G., 1999. Uptake and fractionation of rare earth elements on hydrothermal plume particles at 9°45′N, East Pacific Rise. Geochimica et Cosmochimica Acta 63, 1709–1722.

Siva Siddaiah, N., Hanson, G.N., Rajamani, V., 1994. Rare earth element evidence for syngenetic origin of an Archean stratiform gold sulfide deposit, Kolar schist belt, South India. Economic Geology 89, 1552–1566.

Su, W.C., Qi, L., Hu, R.Z., Zhang, G.P., 1998. Analysis for rare earth elements in fluid inclusions. Science Bulletin 43, 1094–1098 (in Chinese).

Sun, X.L., Liu, X.D., Gao, Z.K., Qian, W.G., Ran, D.F., 2001. A study of the geology and geochemistry of altered rocks from Liba gold deposit in Gansu. Journal of Chengdu University of Technology 28, 350–354 (in Chinese with English abstract).

Taylor, S.R., McLennan, S.M., 1985. The Continental Crust: Its Composition and Evolution. Blackwell, Oxford. 312 pp.

Taylor, S.R., McLennan, S.M., 1995. The geochemical evolution of the continental crust. Reviews in Geophysics 33, 241–265.

Taylor, S.R., Rudnick, R.L., MeLennan, S.M., Erikson, K.A., 1986. Rare earth element patterns in Archean high-grade metasediments and their tectonic significance. Geochimica et Cosmochimica Acta 50, 2267–2279.

Van Middlesworth, P.E., Wood, S.A., 1998. The aqueous geochemistry of the rare earth elements yttrium: Part 7. REE, Th and U contents in thermal springs associated with the Idaho batholith. Applied Geochemistry 13, 861–884.

Wendlandt, R.F., Harrison, W.J., 1979. Rare earth partitioning between immiscible carbonate and silicate liquids and CO_2 vapor: results and implications for the formation of light rare earth-enriched rocks. Contributions to Mineralogy and Petrology 69, 409–419.

Whitehead, R.E., Davies, J.F., Valdes-Nodarse, E.L., Diaz-Carmona, A., 1996. Mineralogical and chemical variations, Castellanos shale-hosted Zn–Pb–Ba deposi, Northwestern Cuba. Economic Geology 91, 713–722.

Wood, S.A., 1990a. The aqueous geochemistry of the rare earth elements and Y: 1. Review of available low-temperature data for inorganic complexes and the inorganic REE speciation of natural waters. Chemical Geology 82, 159–186.

Wood, S.A., 1990b. The aqueous geochemistry of the rare earth elements and Y: 2. Theoretical predictions of speciation in hydrothermal solutions to 350°C at saturation water vapor pressure. Chemical Geology 88, 99–125.

Wu, S.L., Zhao, Y.H., Feng, X.B., 1996. Application of inductively coupled plasma mass spectrometry for total metal determination in silicon-containing solid samples using the microwave-assisted nitric acid–hydrofluoric acid–hydrogen peroxide–boric acid digestion system. Journal of Analytical Atomic Spectrometry 11, 287.

Yang, X., 1985. On the origin of the Woxi Au–Sb–W deposit in Hunan Province. Unpublished M.Sc. thesis, Chengdu College of Geology, Chengdu. 107 pp. (in Chinese).

Yang, X., 1992. Source of ore material and paragenesis of ore building elements in Woxi Au–Sb–W deposit, Hunan. Journal of the Chengdu College of Geology 19 (2), 20–28 (in Chinese with English abstract).

Zhang, Z.R., 1980. The genesis and ore-forming mechanism of the Woxi Au–Sb–W deposit, Taoyuan. Science Information of the Metallurgical Institute of South China 1–10 (in Chinese).

Zhang, Z.R., 1989. Research on Gold Deposits. Press of China Industrial University, Changsha. 190 pp. (in Chinese).

Zheng, M.H., 1989. An Introduction to Stratabound Gold Deposits. Chengdu University of Science and Technology Press, Chengdu. 260 pp. (in Chinese).